# Detailed Characterization of CZT Detector Response for Improved Coded-Aperture Imaging Performance

J. Daughhetee,[1] K-P. Ziock,[1] K. Schmitt,[1] F. Gonzalez,[1] V. Nwadeyi,[2] D. Goodman,[3] and W. Kaye[3]

[1]*Oak Ridge National Laboratory, Oak Ridge, TN 37831, USA*

[2]*Savannah River National Laboratory, Jackson, SC 29831, USA*

[3]*H3D, Inc., Ann Arbor, MI 48108, USA*

Gamma-ray imaging is a powerful method for locating and quantifying sources of radiation. The coded-aperture technique demonstrates superior angular resolution in comparison to other methods (e.g., Compton reconstruction). In this method, a mask constructed of highly attenuating material encodes the scene as a shadow pattern on a position-sensitive detector; this pattern can then be used to recreate the origin(s) of incident radiation. This is typically done through convolution of the mask and shadow patterns. Iterative methods which attempt to reconstruct the observed shadow pattern using a weighted combination of simulated patterns may also be employed. In either case, errors in event position reconstruction due to detector imperfections alter the shadow pattern and will therefore degrade system performance and may introduce imaging artifacts. These effects can be mitigated with a detailed understanding of such errors – allowing for the generation of representative simulations that include the errors and/or correction of raw imager data to remove the errors. We present a calibration process for a commercially available cadmium zinc telluride (CZT) gamma imager which provides a comprehensive characterization of the spatial and energy dependence of event reconstruction. By illuminating a mask featuring a regular grid of pinholes with a calibration source, the localized response of the detector can be measured with fine granularity. These local responses are combined to generate a full detector response map which can be used to distort simulations in a manner that is representative of the observed detector data. Details of the calibration procedure and an assessment of the impact of its end products on the performance of iterative imaging methods will be presented.

Keywords: gamma-ray imaging, coded-aperture, CZT, calibration

## I. INTRODUCTION

For any facility in which nuclear material is processed, monitoring for holdup, the accumulation of material in processing infrastructure, is essential for both material accounting and operational safety. The standard holdup monitoring process uses spectroscopic measurements of gamma-rays at locations suspected of having a high propensity to form deposits [1]. In order to obtain a quantifiable estimate of the holdup mass, assumptions must be made on the distance to and extent of the deposit. Contributions from other sources in the room may also add backgrounds to the measurement that are difficult to disentangle. Coded-aperture imaging can alleviate the impact of some of these uncertainties by providing the ability to better localize and isolate radiation sources of interest. This technique uses a mask populated with opaque and open pixels located in front of the imager to encode a shadow pattern upon the surface of a position-sensitive detector. The distribution of source material within the field of view can then be reconstructed by cross-correlating the observed shadow pattern with the known mask pattern [2]. Applications of this method to measurements of nuclear material have demonstrated that it is capable of producing accurate, quantifiable results [3].

The advantages coded-aperture imaging provides has motivated the development of new holdup measurement systems with the potential to reduce uncertainties on material mass estimates. Specifically, a system featuring multiple copies of a commercially available imager that feature overlapping coded-aperture fields of view has been proposed as a method for automated holdup measurements within a shielded glove box [4]. The system will employ multiple H3D, Inc. model H420 gamma-ray imagers. This imager features four 2.2 x 2.2 x 1 cm CZT crystals and an internal coded-aperture mask (a rank 19 modified uniformly redundant array (MURA)) [5]. These detectors feature an event spatial resolution ($\sim$ 0.5 mm) sufficient for resolving the mask shadow pattern. However, calibration measurements have revealed that there can be significant spatial variations in the position reconstruction. These deviations from nominal detector behavior can introduce imaging artifacts that may affect source location and overall normalization. Understanding these detector imperfections is therefore critical to meeting quantification accuracy and uncertainty targets. Furthermore, these variations are unique between imagers indicating that they originate from defects within the component CZT crystals. To address this issue, a calibration routine has been developed so that individual imagers can be systematically characterized prior to integration with

the full holdup imaging system.

## II. CALIBRATION SETUP

Mapping the spatial variations of the detector response requires well-localized illumination of the detector crystals with a mono-energetic gamma-ray source in a controlled geometry. This mapping is accomplished via the use of a pinhole mask made of tungsten (3-8 mm thick depending on the energy of the incident radiation) which covers the full front face of the detector. The mask is populated with a $15 \times 15$ grid of 750 $\mu$m pinholes which allows the transmission of gamma rays originating from a calibration source placed approximately 1 meter away. Prior to undertaking these measurements, the internal coded-aperture mask is removed. Figure 1 provides a view of the setup from the perspective of the calibration source as well as an example pinhole pattern on the detector. The 3.18 mm spacing of the pinholes ensures that the illumination spots on the detector can be separately resolved. In order to fully examine the face of the detector, the mask is scanned in the horizontal and vertical directions in steps of 0.5 mm with a full measurement set comprising 64 scan locations.

To account for inconsistency in the size of the pinholes, an additional measurement is taken wherein all but 1 of the pinholes for a given detector quadrant is blocked by a secondary mask. The mask is then scanned so that a normalization measurement can be obtained for every pinhole. Finally, four measurements of the same pinhole are taken in each of the detector quadrants to account for differences in efficiency between crystals.

## III. DETECTOR CHARACTERIZATION

A complete pinhole scan dataset provides information on how events are reconstructed across the face of the detector with fine granularity. For this proceeding, pinhole scans using $^{57}$Co and $^{133}$Ba sources are analyzed using two different approaches. The methods are primarily evaluated by how well they reconcile differences between simulation and measured data.

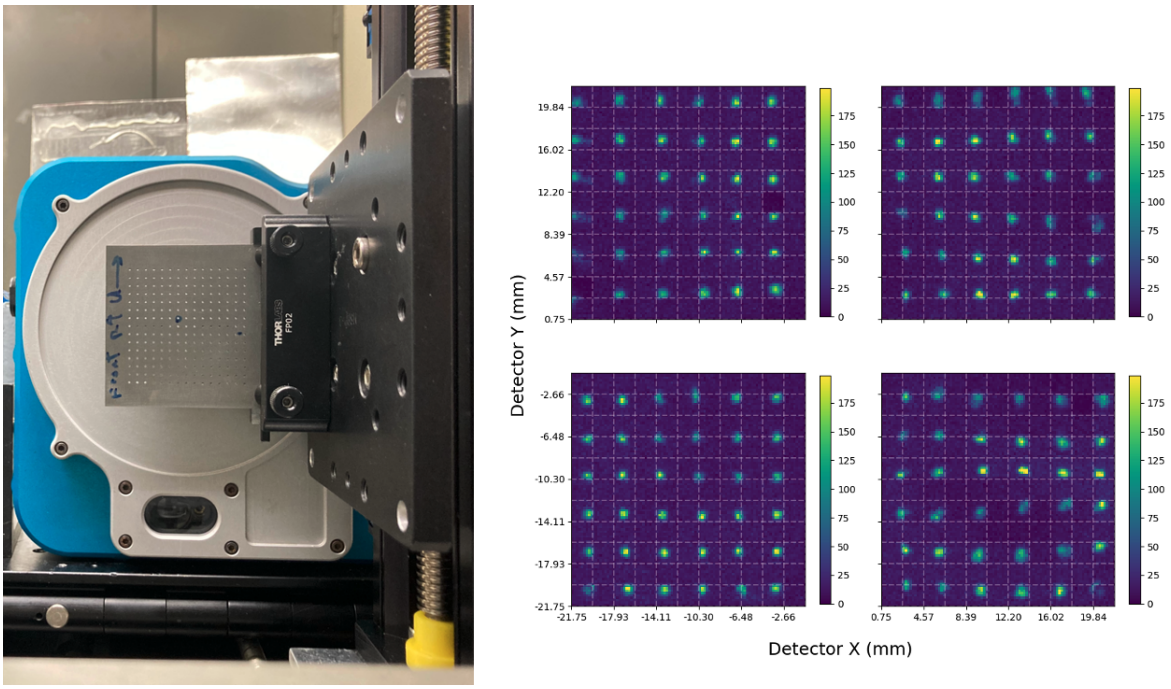


Fig. 1: (Left) Photograph of the measurement setup form the view of the calibration source. (Right) Reported event locations for $^{133}$Ba source data acquired with the pinhole mask in place. Close examination of the pinhole spacing reveals the deformation of the uniform grid.

### A. Detector Linearization

The first approach is to develop a transform from the 'electronic' event location to the true physical location so that data can be corrected. For this analysis, the detector data are finely binned ($180 \times 180$) in the x and y coordinates. To determine the location of the pinholes in electronic space, single rows and columns of pinhole data are collapsed into one dimension and both the mean of a Gaussian fit and the centroid of the distribution are calculated (Fig 2). The implementation of two methods in the process is necessitated by occasional instances of unusual morphology in the distributions. Any pinholes for which the result of the two methods differed by more than 190 $\mu$m are flagged, and the analyst can make a determination on the more appropriate method.

The set of all spot locations are then ordered by their true physical locations, and any points whose location is not at least 0.2 bins greater than the preceding point are trimmed from the set. This removes regions where crystal defects impart a large effect or where two separate physical locations map to the same electronic position. The resulting matrix is an ordered set of electronic locations linked to physical locations whose positions are monotonically increasing with a regular

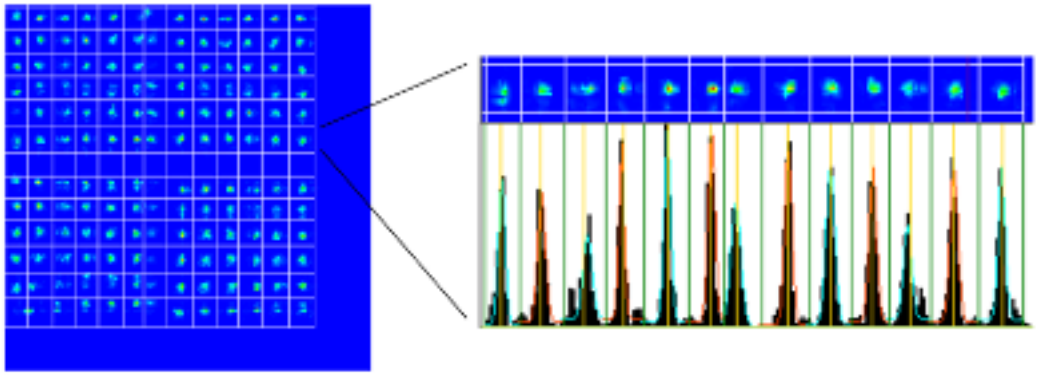

Fig. 2: (Left) Pinhole data for a $^{57}$Co measurement. (Right) Zoomed image of one row of pinholes with with an accompanying projection onto the x-axis. Centroids of the distributions are given by the gold line while the Gaussian fit is in cyan.

step size. The electronic positions, while monotonically increasing, do not have regular step sizes. This produces a distorted space of linked quadrilaterals as opposed to the square grid of the true locations (Fig 3). A given event's electronic location lies within some quadrilateral defined by four points in the matrix each connected by line segments. If this location is redefined as a fractional distance along the bounding line segments, then the corresponding location in the non-distorted physical space can be determined. To save on computational expense, a one-time calculation is performed on a grid of regularly spaced electronic positions to create a matrix of real-world positions. This matrix can then be applied to detector data to transform from electronic to physical coordinates.

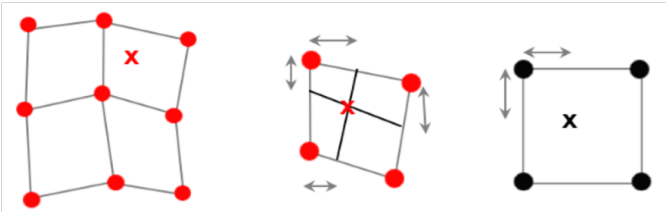

Fig. 3: An example diagram showing how an event location in electronic space (red) maps to the physical space defined by the pinhole scan (black).

Application of this matrix to sample pinhole data (Fig 4) demonstrates that this method is effective in regularizing the pinhole locations. The matrix was also applied to data acquired while the detector was uniformly illuminated with a $^{57}$Co source and no mask. The correction intro-

duced a significant amount of structure in the flat-field event distribution. To prevent this structure from manifesting as artifacts in the coded-aperture images, an efficiency map is generated from the flat-field data that can then be applied to other measurements prior to generating images.

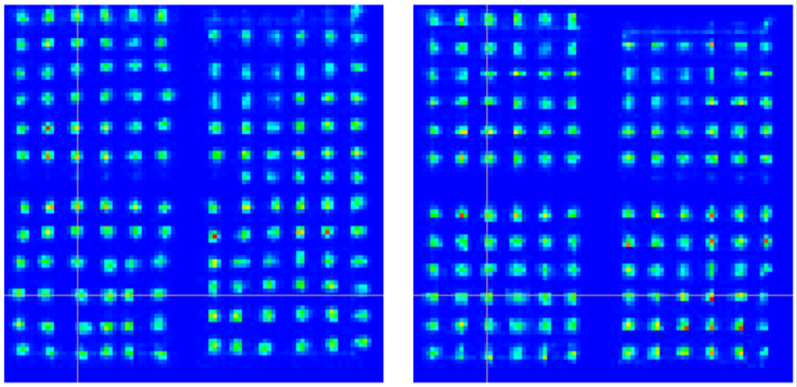

Fig. 4: Example pinhole data prior to application of the correction matrix (left) and after correction (right). Examination of the pinhole spots with relation to the cursor lines in the image show the improved regularity of the grid.

The primary benefit of this data correction approach is that it circumvents the need to generate highly tailored simulations for specific detectors. This is highly relevant for proposed iterative image reconstruction methods which require a large set of simulations to function effectively [6]. To determine how well the data and simulation agree, we examine the coded-aperture imaging efficiency across the field of view. Efficiency maps for uncorrected data, simulation, and corrected data are shown in Figure 5. While there is some improvement in agreement after application of the linearization matrix, there are still some discrepancies (particularly in the corners of the central part of the map). It is suspected that the discrepancies are largely due to the correction method excluding highly distorted regions of the detector.

### B. Response Model

Rather than correcting the data as reported by the detector, one can also consider constructing a model of the detector response that can be used to perturb ideal simulated data so that it will match observations. This model consists of a collection of event distributions in detector space that correspond to known physical locations as defined by the pinhole scan. Simulation events can then be 'pushed' by finding the nearest pinhole measurement and probabilistically sampling its

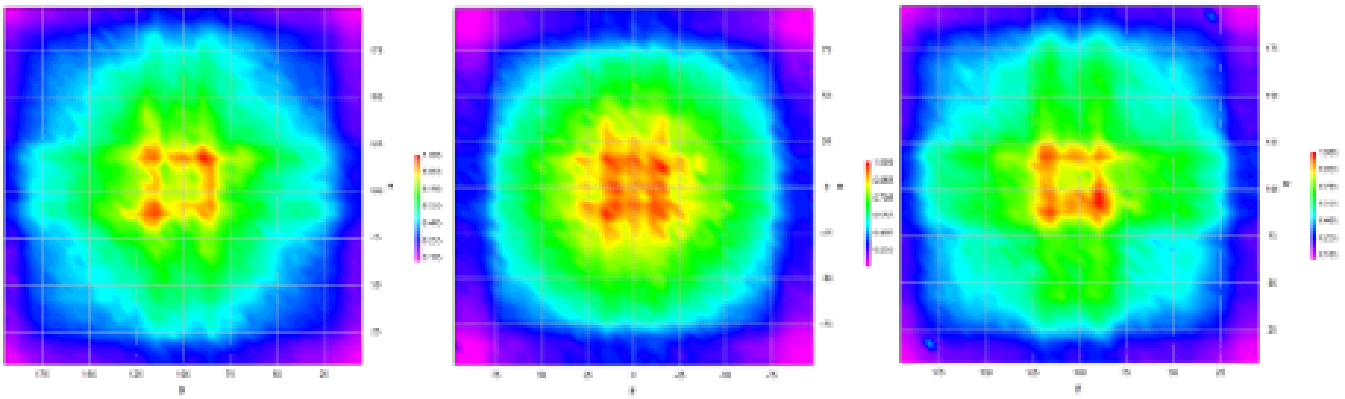

Fig. 5: Field-of-view efficiency maps for an H420 imager at 122 keV generated from detector data (left), simulated data with Gaussian blurring applied (middle), and corrected detector data (right).

event distribution. The end result is a set of simulation data that emulates the observed detector data.

The first step in the construction of this model is to finely bin the detector data ($198 \times 198$) to create a two-dimensional histogram of hit locations within a specified energy window. For each known pinhole location, a search is performed within a limited radius to find an event cluster associated with that pinhole. If a cluster is found, a subset of the histogram data centered about the cluster location is selected. To reduce background noise, any bins in this subset featuring fewer than 10% of the events in the maximum bin are set to zero. The remaining non-zero bins in the subset are then normalized by measurement livetime and serve as a probability distribution function (PDF) for the associated pinhole (Fig 6). Lastly, the bins used in the PDF are subtracted from the original $198 \times 198$ data histogram so that they cannot be attributed to another pinhole location.

The output of this process is a large set $\mathcal{O}(10^4)$ of response maps, pinhole locations and their associated event distributions in electronic space. Additionally, because the counts per unit livetime are also tracked, the relative detection efficiency of each of these locations is known as well. These efficiency values will only be valid, however, if the size of all pinholes in the mask is consistent. The potential for significant variations in pinhole size motivated the additional pinhole normalization measurement described in Section II. After applying the results of this measurement to the set of relative efficiencies, a complete response model is obtained. These response models can be visualized as 'push' maps, i.e., a field of arrows connecting the true pinhole location to the average

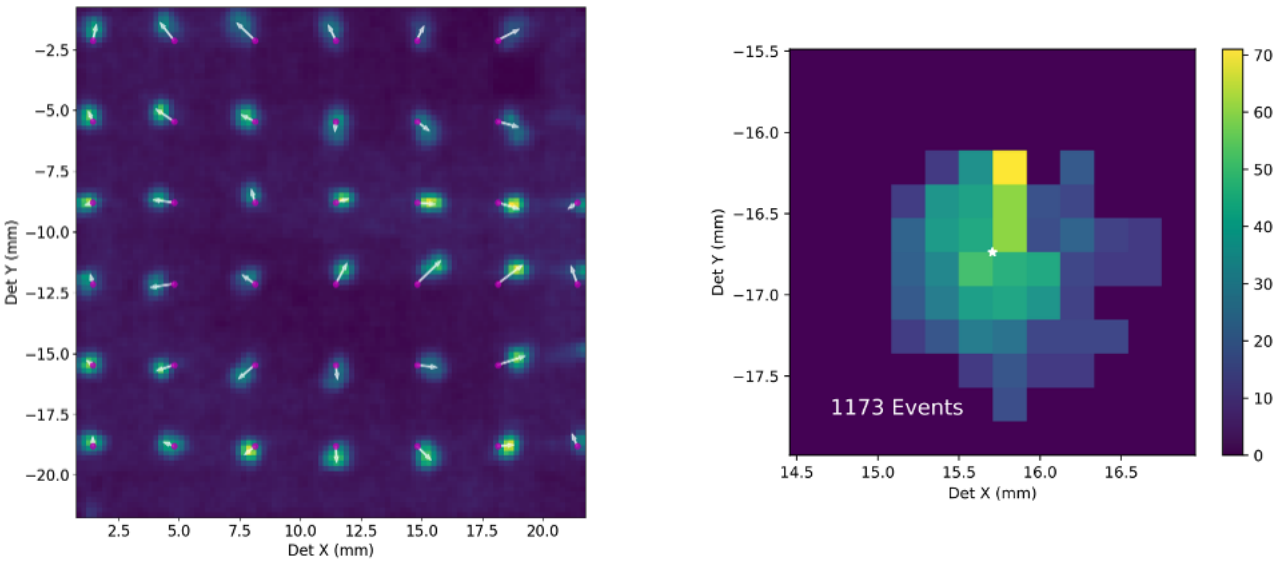


Fig. 6: (Left) Pinhole event distribution for a single CZT crystal for a $^{133}$Ba source at 356 keV. The true pinhole locations are overlaid in magenta. An arrow links the true pinhole location to the mean of the associated distribution. (Right) An example pinhole spot after setting sub-threshold bin values to zero. This distribution is used to form a PDF for the associated pinhole location.

position of its corresponding PDF (Figure 7). These maps are useful in visualizing how defects in the CZT crystal impact the drifting of charge through the bulk.

The application of the detector response model to simulated data is straight-forward. First, the response map closest to the simulated event's position $\overrightarrow{r}$ is identified. Next, the PDF for that response map is sampled to obtain an new event location $\overrightarrow{p}$. Lastly, a translation to account for the lateral offset between $\overrightarrow{r}$ and the position of the response map is applied to $\overrightarrow{p}$ to obtain a response adjusted position $\overrightarrow{r_{adj}}$. Field-of-view efficiency maps generated with measurement data and model-adjusted simulated data are shown in Figure 8. Although some subtle differences between the two remain, the overall level of agreement is much improved.

While the response model method provides much better data-simulation agreement, it is not without its disadvantages. Obtaining accurate efficiency measurements requires longer pinhole calibration measurements to prevent statistical uncertainties from dominating. In the context of iterative imaging, the response must be applied to the full set of simulations used as a basis for reconstruction as opposed to simply applying the detector correction matrix to measured data. Fortunately, the computational cost for doing so does not appear to be prohibitive.

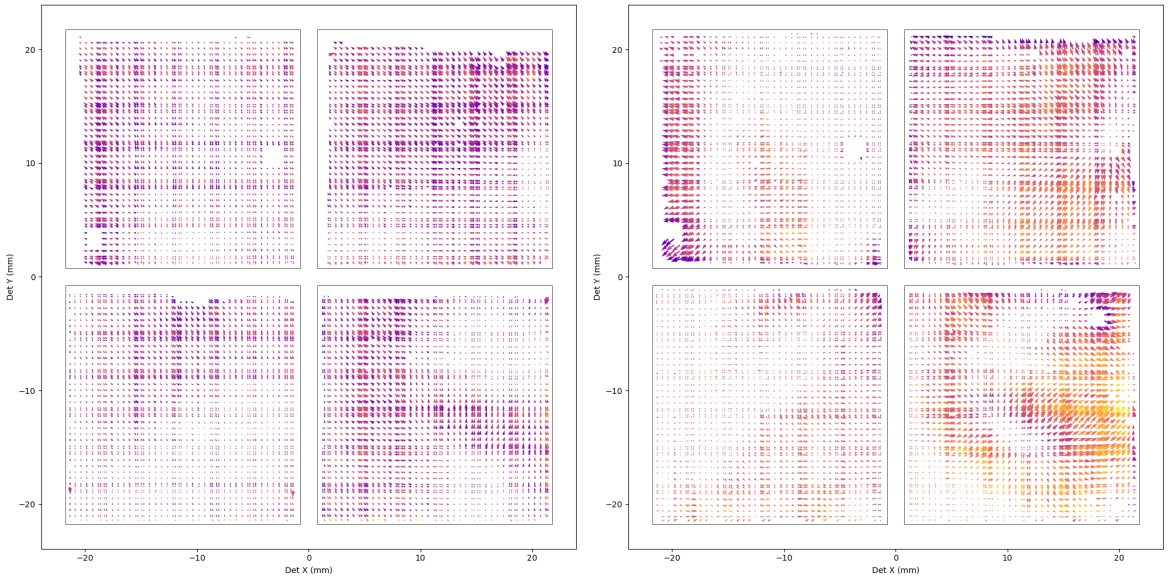


Fig. 7: Distortion maps generated from pinhole scan data at 122 keV (left) and 356 keV (right) using $^{57}$Co and $^{133}$Ba sources respectively. The length of the arrows directly corresponds to the magnitude of the lateral offset while the color reflects the relative efficiency of that location. Some large-scale features can be seen in both maps, however the reconstruction performance at 122 keV appears to wash out features that are more distinct at 356 keV.

## IV. SUMMARY

A radiation imaging system composed of multiple coded-aperture CZT gamma imagers is presently being developed to address the challenge of locating and quantifying holdup material. This system will use iterative reconstruction methods that make use of large sets of simulation data. Achieving accurate results will therefore require simulation and observation to be in good agreement. Initial attempts to rectify differences between simulation and laboratory measurements revealed that simple detector resolution models were not adequate, thereby requiring the development of a detailed calibration method.

A repeatable calibration process was devised in which a pinhole mask is used to probe spatial variations in the detector response. Data from these measurements are analyzed using two approaches: one in which detector data are corrected and one in which simulation is distorted. The method in which a detector response is applied to simulation data was demonstrated to produce superior data-simulation agreement. The process is also highly automated which renders it repeat-

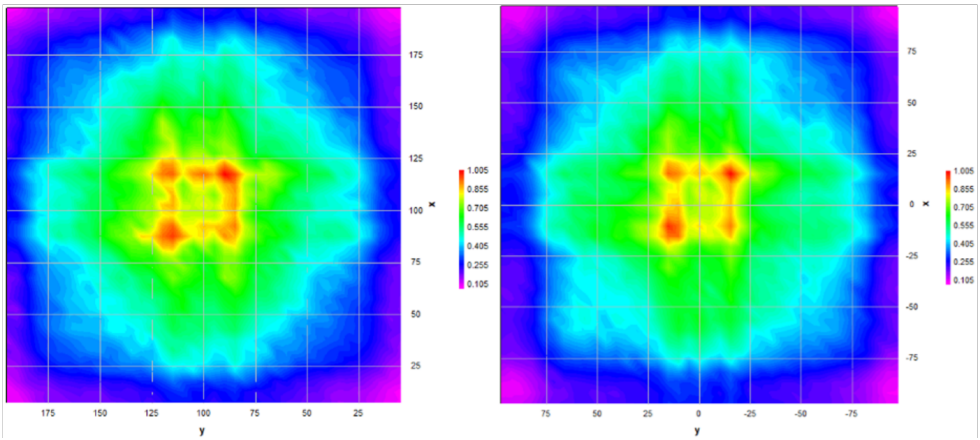


Fig. 8: Field-of-view efficiency maps for at 122 keV for detector data (left) and simulated data that has been adjusted using the response model (right).

able and lessens the burden of obtaining characterizations for additional imagers. Additional steps to be taken include improved measurement alignment control and implementation of a method for modeling the response at intermediate energies where there is a lack of useful calibration sources. Completion of this last task will allow the system to obtain improved quantification results over a wide range of applications.

---

[1] Russo, P A, Wenz, T R, Smith, S E, and Harris, J F. "Achieving Higher Accuracy in the Gamma-Ray Spectrocopic Assay of Holdup," United States: N. p., 2000. Web. doi:10.2172/775830.

[2] E.E. Fenimore, T.M. Cannon, “Coded aperture imaging with uniformly redundant arrays,” Applied Optics, 17, 337-347, 1978.

[3] Klaus-Peter Ziock, et al., "Quantitative Holdup Determination Using Coded-Aperture Gamma-Ray Imaging," INMM Meeting Proceedings 2021

[4] Kyle Schmitt, et al., "Progress Toward Gamma-Ray Imaging for Automated Holdup Measurement in Gloveboxes," INMM Meeting Proceedings 2024

[5] H3D H420 Gamma-ray Imaging Spectrometer, https://h3Dgamma.com/H420Specs.pdf, accessed: 2024-05-01

[6] A. Laminack, et al., "3D Source Reconstruction Using Coded Aperture Gamma-Ray Imaging," INMM Meeting Proceedings 2023